Meteoritics & Planetary Science 41, Nr 6, 851–862 (2006)
Abstract available online at http://meteoritics.org

Cosmic-ray exposure age and heliocentric distance of the parent bodies of enstatite chondrites ALH 85119 and MAC 88136

D. NAKASHIMA[1†*], T. NAKAMURA[2], and R. OKAZAKI[2]

[1]Department of Earth and Planetary Sciences, Graduate School of Sciences, Kyushu University, Hakozaki, Fukuoka 812-8581, Japan
[2]Department of Earth and Planetary Sciences, Faculty of Sciences, Kyushu University, Hakozaki, Fukuoka 812-8581, Japan
[†]Present address: Max Planck Institute for Chemistry, D-55128 Mainz, Germany
[*]Corresponding author. E-mail: naka@mpch-mainz.mpg.de

(Received 26 May 2005; revision accepted 17 February 2006)

Abstract–We measured concentrations and isotopic ratios of noble gases in enstatite (E) chondrites Allan Hills (ALH) 85119 and MacAlpine Hills (MAC) 88136. These two meteorites contain solar and cosmogenic noble gases. Based on the solar and cosmogenic noble gas compositions, we calculated heliocentric distances, parent body exposure ages, and space exposure ages of the two meteorites. The parent body exposure ages are longer than 6.7 Ma for ALH 85119 and longer than 8.7 Ma for MAC 88136. The space exposure ages are shorter than 2.2 Ma for ALH 85119 and shorter than 3.9 Ma for MAC 88136. The estimated heliocentric distances are more than 1.1 AU for ALH 85119 and 1.3 AU for MAC 88136. Derived heliocentric distances indicate the locations of parent bodies in the past when constituents of the meteorites were exposed to the Sun. From the mineralogy and chemistry of E chondrites, it is believed that E chondrites formed in regions within 1.4 AU from the Sun. The heliocentric distances of the two E chondrite parent bodies are not different from the formation regions of E chondrites. This may imply that heliocentric distances of E chondrites have been relatively constant from their formation stage to the stage of exposure to the solar wind.

INTRODUCTION

Enstatite (E) chondrites are the highly reduced group of chondrites. The highly reduced characteristics of E chondrites likely indicate their formation in the inner region of the solar nebula (Kallemeyn and Wasson 1986). Larimer and Anders (1967) conclude that E chondrites formed in the inner fringes of the asteroid belt. Specific locations range within 1 AU from the Sun (Baedecker and Wasson 1975) and in regions near the orbit of Mercury (Sears 1980). The oxygen isotopic compositions of E chondrites are similar to those of the Earth and the Moon (Mayeda and Clayton 1980; Clayton and Mayeda 1985; Clayton et al. 1984; Ivanov et al. 1987; Newton et al. 2000). This may also imply formation in the inner regions of the solar nebula. Lugmair and Shukolyukov (1998) found a correlation between relative abundances of radiogenic ^{53}Cr in solar system objects and their heliocentric distances. From this correlation and the relative abundance of radiogenic ^{53}Cr in E chondrites, Shukolyukov and Lugmair (2004) recently inferred that E chondrites formed within 1.4 AU. Thus, formation regions of E chondrites are considered to be in zones closer to the Sun than the asteroid belt.

Few studies have attempted to quantitatively estimate heliocentric distances of E-chondrite parent bodies. Gas-rich brecciated meteorites are available for such a quantitative estimation. The brecciated meteorites show characteristic light-dark structures composed of coarse-grained "light" and fine-grained "dark" portions. The dark portions contain solar and cosmogenic noble gases (Suess et al. 1964; Signer 1964), which is indicative of direct exposure to the Sun. The light portions contain only cosmogenic gases, indicating shielding from solar radiation. It is generally agreed that these brecciated meteorites originate from surface regoliths of parent body asteroids (Wänke 1965; Lal and Rajan 1969; Pellas et al. 1969; Wilkening 1971; Pellas 1972; Schultz et al. 1972; Rajan 1974; Anders 1975; Housen et al. 1979; Keil 1982; Goswami et al. 1984). Noble gases in the brecciated meteorites and the following approach may provide information regarding heliocentric distances of the meteorite parent bodies at the time when constituents of the meteorites were exposed to the Sun.

The surficial regions of the regolith are exposed to solar winds (SW), solar energetic particles (SEP), and galactic cosmic rays (GCR). The SW penetrates to several hundred Ångströms and SEP from millimeters to centimeters below

the surface (Walker 1980), and are implanted directly on mineral grains residing on the surface. Their fluxes are inversely related to the square of the heliocentric distance. The GCR penetrates ~1 m or so (Walker 1980) and produces cosmogenic noble gases via spallation reactions with target elements. Since the GCR flux is assumed to be constant in the whole solar system, the production of cosmogenic gases is independent of the heliocentric distance. GCR exposure ages can be calculated from the cosmogenic gas concentrations. Cosmogenic gases are also produced by the higher-energy component of the SEP (i.e., solar cosmic rays). Solar cosmic rays (SCR) produce cosmogenic gases in the top few centimeters of the regolith. Although SCR production rates for cosmogenic nuclides are high relative to the GCR production rates, regolith mixing processes (Housen et al. 1979) continuously mix surface grains into lower regions of the regolith. Following Wieler et al. (1989), we assume that the SCR contribution can be neglected. The concentration of solar noble gas implanted per unit time (solar gas implantation rate) is inversely related to the square of heliocentric distance, because fluxes of SW and SEP are inversely proportional to the square of the heliocentric distance. The heliocentric distance of the meteorite parent body is obtained by comparison between the solar gas implantation rate of the meteorite and that of lunar samples, because the Moon is known to be located at 1 AU. Since the concentration of solar noble gases varies both with exposure time and heliocentric distance, it is difficult to estimate the exposure duration from solar gas concentration. However, some meteorites do show a correlation between solar gas concentrations and GCR exposure ages (e.g., Anders 1975). Anders (1975) interpreted the ratios of solar gas concentrations to GCR exposure ages in these meteorites as solar gas implantation rates and used them to estimate heliocentric distances of meteorite parent bodies (carbonaceous and ordinary chondrites, and also howardites). This estimation is based on the assumption that the ratio of the SW/SEP exposure duration to GCR exposure age is similar for the Moon and meteorite parent body surfaces. Based on comparison to lunar materials, Anders (1975) reasoned that an upper limit to the location of exposure is 8 AU. Anders (1975) could not give a more constrained estimate (the upper limit could be as low as 4 AU) because it was not possible to resolve cosmogenic noble gases produced on parent bodies from those produced during the meteoroid exposure. Wieler et al. (1989) and Nakashima et al. (2002) used an extended approach to distinguish between parent body and meteoroid exposure, and derived distances of ordinary chondrite parent bodies from the Sun. However, heliocentric distances of E chondrite parent bodies have never been estimated.

The purpose of this study is to determine heliocentric distances and the parent body exposure ages of E chondrites to reveal the orbits and regolith evolution of E chondrite parent bodies. We prepared small chips from two solar gas-bearing EL3 chondrites: Allan Hills (ALH) 85119 and MacAlpine Hills (MAC) 88136 (Patzer and Schultz 2002). Concentrations of solar ^{36}Ar ($^{36}Ar_S$) and cosmogenic ^{21}Ne ($^{21}Ne_C$) in many pieces of the two meteorites were determined by noble gas analyses. Heliocentric distances, parent body exposure ages, and space exposure ages of the two meteorites were calculated.

EXPERIMENTAL PROCEDURES

Although ALH 85119 and MAC 88136 are solar-gas-bearing meteorites (Patzer and Schultz 2002), they do not exhibit a light-dark structure. This may be due to terrestrial weathering effects (limonitic staining). Meteorite samples were crushed into small pieces, weighing from 0.3 to 2.2 mg, to see variations in concentrations of $^{36}Ar_S$ and $^{21}Ne_C$. Each sample was heated to 1700 °C. Concentrations and isotopic ratios of He, Ne, and Ar were measured with a noble gas mass spectrometer (Nakamura et al. 2003). Concentrations of ^{84}Kr and ^{132}Xe were also measured.

Trapped and cosmogenic components of He, Ne, and Ar were separated based on their isotopic ratios. E3 chondrites are known to contain primordial gases enriched in Xe (sub-Q; $^{36}Ar/^{132}Xe$ ~37) (Patzer and Schultz 2002), which are believed to originate from fractionation of Q gases. The $^{4}He/^{20}Ne/^{132}Xe$ ratios of sub-Q gases are not known. Following Busemann et al. (2000), we assume that the $^{4}He/^{20}Ne/^{132}Xe$ ratios are ~374/3.2/1; however primordial ^{4}He and primodial ^{20}Ne concentrations are only ~1% of trapped ^{4}He and trapped ^{20}Ne concentrations. The percentages must be lower than 1% if sub-Q gases are formed by larger depletions of lighter elements relative to Xe from Q-gases. Unlike He and Ne, primordial Ar may account for some part of trapped Ar in the two E chondrites. The $^{36}Ar_S$ concentrations were obtained by subtracting primordial ^{36}Ar concentrations from those of trapped ^{36}Ar where primordial ^{36}Ar concentrations were obtained based on measured ^{132}Xe concentrations. For the correction, a $(^{36}Ar/^{132}Xe)_{primordial}$ value of 28.6 was assumed for ALH 85119, which is the ratio between concentrations of trapped ^{36}Ar and ^{132}Xe in the solar-gas-poor sample (ALH 85119: A3 in Appendix 1). The $(^{36}Ar/^{132}Xe)_{primordial}$ for MAC 88136 was assumed to be 37.3, from the solar-gas-free EL3 chondrite MAC 88184 paired with MAC 88136 (Patzer et al. 2001), because heavy noble gases in a solar-gas-poor sample of MAC 88136 could not be measured.

RESULTS

Figure 1 shows a Ne three-isotope diagram. Ne isotopic ratios are distributed in an area defined by Ne SW, Ne SEP, and Ne cosmogenic, showing that the Ne in the individual samples is the mixture of solar Ne and cosmogenic Ne. This is consistent with the previous results of Patzer and Schultz (2002). The presence of solar gases indicates that constituents of the two meteorites had been exposed to solar wind particles on the surface of the parent bodies.

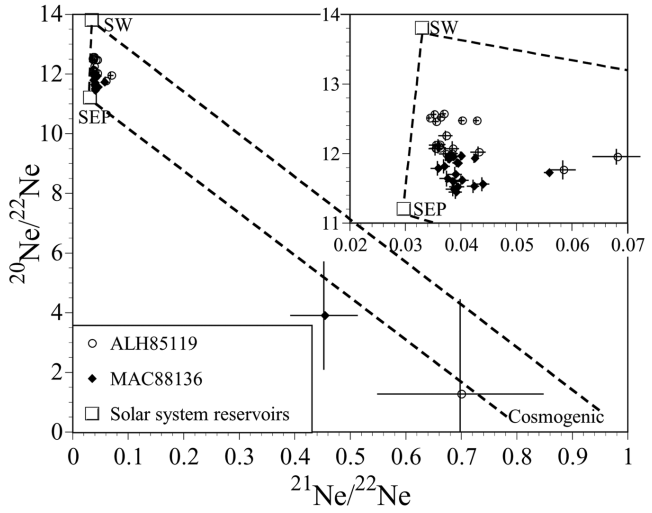

Fig. 1. A Ne three-isotope diagram showing Ne data of many pieces of ALH 85119 and MAC 88136. Ne isotopic ratios of solar wind ($^{20}Ne/^{22}Ne$, $^{21}Ne/^{22}Ne)_{SW}$ = (13.8, 0.0328) and solar energetic particles ($^{20}Ne/^{22}Ne$, $^{21}Ne/^{22}Ne)_{SEP}$ = (11.2, 0.0295) are given by Benkert et al. (1993).

The $(^4He/^{20}Ne)_S$ ratios of ALH 85119 (49.6 ± 5.4 on average) and MAC 88136 (104 ± 6 on average) are lower than the typical value for solar-wind-implanted species ($^4He/^{20}Ne$ = 253 ± 10 for lunar soil ilmenites 12001) (Eberhardt et al. 1972). There are two possible explanations for the low $(^4He/^{20}Ne)_S$ ratios: ^4He_S saturation and ^4He_S diffusive loss. If the low $(^4He/^{20}Ne)_S$ ratios are due to ^4He_S saturation, $(^4He/^{20}Ne)_S$ ratios decrease with increasing $^{20}Ne_S$ concentrations. However, such an inverse correlation is not observed (Fig. 2a). Hence, it is more likely that the low $(^4He/^{20}Ne)_S$ ratios are due to ^4He_S diffusive loss. The $(^{20}Ne/^{36}Ar)_S$ ratios and $^{36}Ar_S$ concentrations show no inverse correlation either (Fig. 2b), which indicates neither $^{20}Ne_S$ nor $^{36}Ar_S$ are in saturation. The $(^{20}Ne/^{36}Ar)_S$ ratios of ALH 85119 (34.7 ± 7.8 on average) and MAC 88136 (31.5 ± 2.1 on average) are consistent with the value for lunar soil ilmenites 12001 ($^{20}Ne/^{36}Ar$ = 26.8 ± 5.4) (Eberhardt et al. 1972) within 1σ variations. Although the lunar soil ilmenites 12001 might have lost some Ne, they have not lost Ar (Eberhardt et al. 1972). The same is likely true also for the two meteorites. Thus, elemental ratios suggest that the two E chondrites have lost some He and Ne, but not Ar, and indicate that $^{36}Ar_S$ is not in saturation.

Figure 3 shows correlations between concentrations of $^{21}Ne_C$ and $^{36}Ar_S$ in the samples of ALH 85119 and MAC 88136 (Table 1). The $^{21}Ne_C$ concentrations correlate also with those of ^4He_S and $^{20}Ne_S$. However, we are focusing on the correlation between $^{21}Ne_C$ and $^{36}Ar_S$ because $^{36}Ar_S$ has not suffered diffusive loss. The interpretation of the correlations is discussed in the next section.

Unlike $^{21}Ne_C$, $^{38}Ar_C$ concentrations do not correlate with solar gas concentrations, which may be due to $^{38}Ar_C$ loss during terrestrial weathering (Okazaki et al. 2000; Patzer and Schultz 2001). Also ^3He_C concentrations and solar gas concentrations do not show correlations, which may be due to ^3He_C diffusive loss.

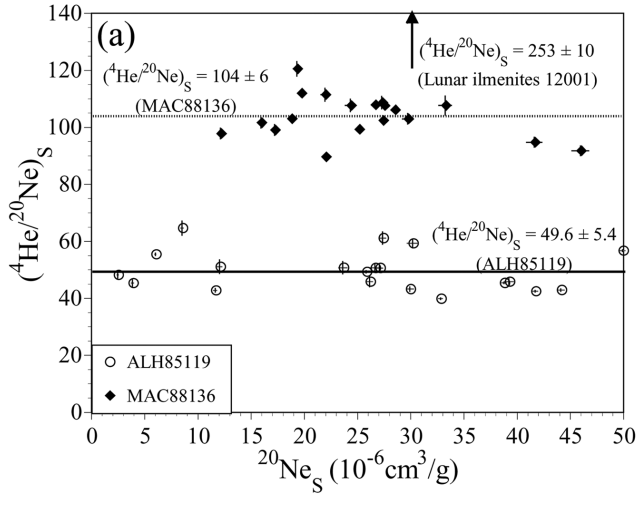

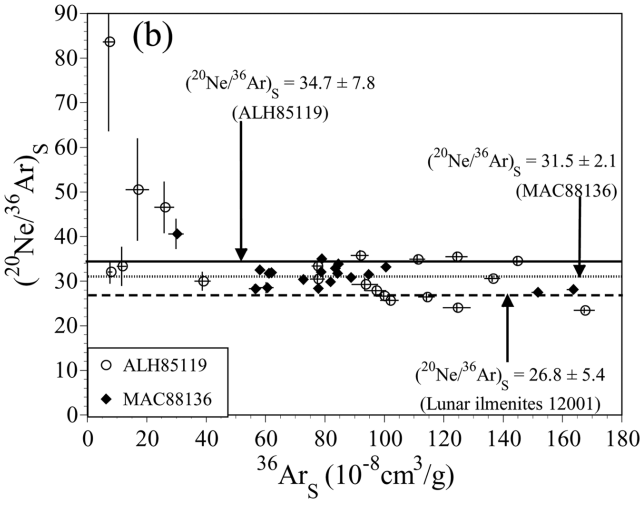

Fig. 2. a) The relationship between $(^4He/^{20}Ne)_S$ and $^{20}Ne_S$. The solid line is the average $(^4He/^{20}Ne)_S$ ratio for samples of ALH 85119, whereas the dotted line is the average $(^4He/^{20}Ne)_S$ ratio for samples of MAC 88136. b) The relationship between $(^{20}Ne/^{36}Ar)_S$ and $^{36}Ar_S$. The solid line is the average $(^{20}Ne/^{36}Ar)_S$ ratio for samples of ALH 85119, whereas the dotted line is the average $(^{20}Ne/^{36}Ar)_S$ ratio for samples of MAC 88136. The dashed line is the $(^{20}Ne/^{36}Ar)_S$ ratio of lunar soil ilmenites 12001 (Eberhardt et al. 1972). Data fall far above the other data might be due to underestimation of $^{36}Ar_S$ by inaccurate correction for primordial ^{36}Ar. In both figures, solar-gas-poor samples are excluded.

INTERPRETATION AND CALCULATION

Interpretation of Figure 3

Wieler et al. (1989) and Pedroni (1991, 1992) found a correlation between solar and cosmogenic gas concentrations in samples from the dark portions of the meteorites. They interpret the correlation as mixtures of irradiated and

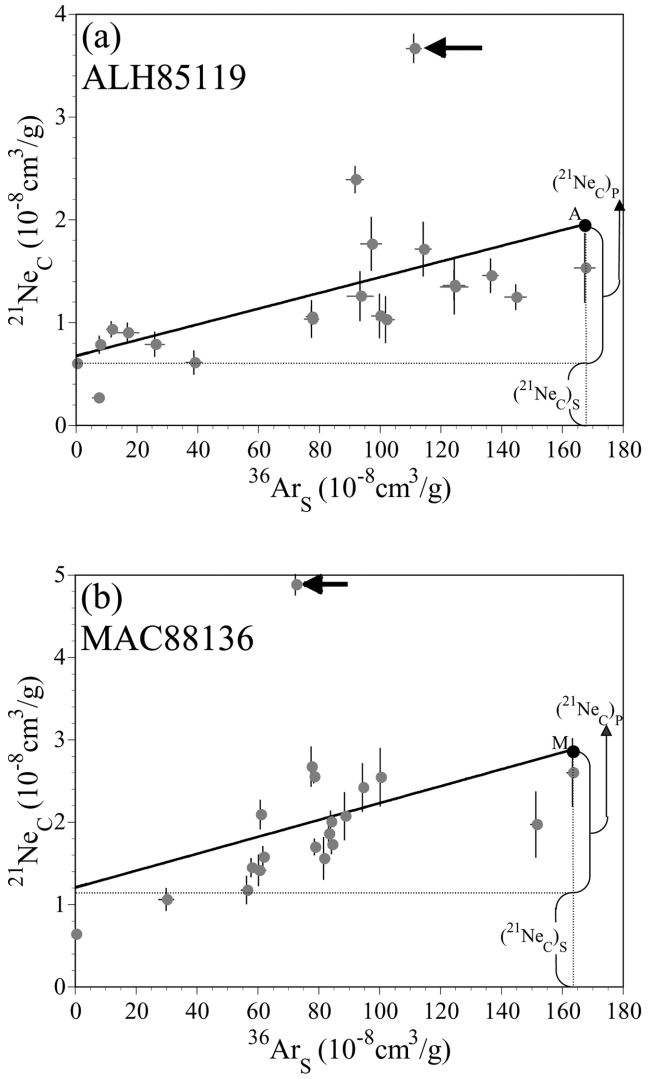

Fig. 3. The relationship between $^{21}Ne_C$ and $^{36}Ar_S$ in ALH 85119 (a) and MAC 88136 (b). The solid lines are the correlation lines for samples of the two meteorites. $(^{21}Ne_C)_P$ corresponds to $^{21}Ne_C$ produced during the parent body exposure, and $(^{21}Ne_C)_S$ corresponds to $^{21}Ne_C$ produced during the space exposure. Points "A" and "M" are defined by the highest $^{36}Ar_S$ concentrations measured in ALH 85119 and MAC 88136, respectively. They correspond to the point for irradiated small grains in Fig. 4c. Data points with large deviations are marked by arrows. They are discussed in the "Results of Calculations and Discussion" section.

Table 1. Concentrations of $^{36}Ar_S$ and $^{21}Ne_C$.

	Sample	$^{36}Ar_S$	$^{21}Ne_C$
		$10^{-8}cm^3/g$	
ALH 85119	A1	77.4	1.04
	A2	99.8	1.07
	A3	n.c.	0.603
	A4	7.64	0.786
	A5	11.5	0.935
	A6	25.8	0.790
	A7	114	1.72
	A8	167	1.53
	A9	97.1	1.77
	A10	102	1.03
	A11	16.8	0.902
	A12	93.4	1.26
	A13	124	1.35
	A14	38.7	0.612
	A15	7.17	0.269
	A16	136	1.46
	A17	145	1.25
	A18	91.7	2.39
	A19	77.3	1.06
	A20	111	3.67
	A21	124	1.36
MAC 88136	M1	81.5	1.56
	M2	151	1.97
	M3	163	2.60
	M4	77.4	2.67
	M5	60.7	2.09
	M6	88.4	2.07
	M7	94.3	2.42
	M8	100	2.55
	M9	56.3	1.18
	M10	60.2	1.42
	M11	n.c.	0.640
	M12	29.8	1.06
	M13	83.1	1.86
	M14	61.6	1.58
	M15	83.8	2.01
	M16	72.3	4.88
	M17	78.5	1.70
	M18	57.7	1.45
	M19	78.3	2.55
	M20	84.1	1.73

n.c. = not calculated; the concentrations of solar Ar are not calculated because of lack of discernible solar gases.

unirradiated grains in various proportions. The former acquires solar and cosmogenic gases during exposure to SW, SEP, and GCR on the parent body surface and to GCR in space. The latter acquires cosmogenic gases by GCR exposure in space only. Although the two E chondrites studied here do not have the classic light-dark structure, the process of mixing irradiated and unirradiated grains is applicable also to the correlation in Fig. 3.

To understand this interpretation, we consider exposure scenarios of four types of materials: irradiated small grains, irradiated fragments, unirradiated small grains, and unirradiated fragments (Fig. 4). The small grains are assumed to have a size of ~50 μm, which is comparable to average grain sizes in the dark portions of solar-gas-bearing meteorites (Eberhardt et al. 1965; Schultz 1973). The fragments are assumed to have a size of ~1 cm, which is a typical size of the light portions (mm–cm; e.g., Housen and Wilkening 1982). In this scenario, we do not include SCR, because it is inferred from a comparison between $^{21}Ne_C$ production rates by GCR and SCR that SCR contribution to $^{21}Ne_C$ production is not significant.

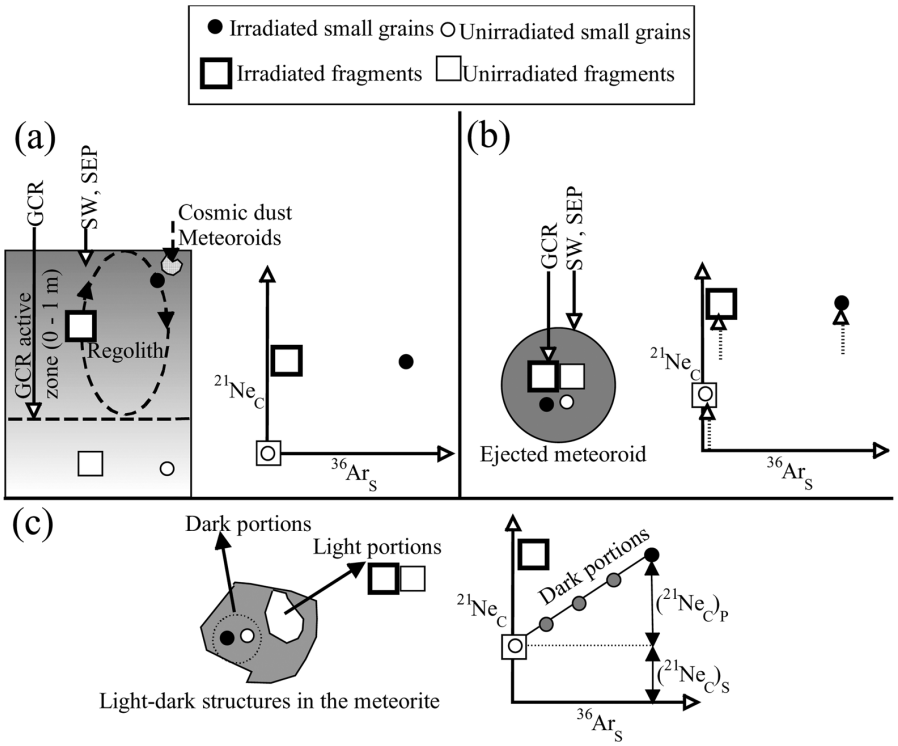

Fig. 4. a) Exposure on the regolith of the meteorite parent body. b) Exposure in space. c) The light-dark structures in the meteorite. In each illustration, the $^{21}Ne_C$-$^{36}Ar_S$ diagram describes concentrations of $^{21}Ne_C$ and $^{36}Ar_S$ in the materials.

Figure 4a shows the appearance of regolith, and the $^{21}Ne_C$-$^{36}Ar_S$ diagram in the figure shows data points expected for the different materials in the regolith. To simplify the scenario, it is assumed that surface regolith is continuously mixed in the 0–1 m depth range (GCR active zone) due to bombardment of cosmic dust and meteoroids and exposed similarly to SW, SEP, and GCR (i.e., well-mixed regolith stratum). Irradiated small grains are plotted as one discrete point in the Ne-Ar diagram (Fig. 4a). On the other hand, irradiated fragments are plotted as one point near the y-axis of the diagram (Fig. 4a), because they cannot acquire high concentrations of solar gases like small grains due to the small surface/volume ratio (200 times less than that of the small grains). Unirradiated small grains and fragments below GCR active zone are plotted on the origin in the diagram (Fig. 4a), because they acquire neither solar nor cosmogenic gases.

After the admixture of unirradiated materials to irradiated materials and residence in a deep site to which even GCR cannot penetrate, all the materials within the meteoroid are ejected from the parent body upon a large-scale impact (Fig. 4b). During transit to the Earth, all materials are then exposed to GCR only. As a result, only the $^{21}Ne_C$ concentration increases, and all data points are shifted upwards in the Ne–Ar diagram (Fig. 4b).

Meteorites that experienced such exposures show the light-dark structure (Fig. 4c). The light portions are equivalent to irradiated and unirradiated fragments, and their data are plotted along the y-axis in the Ne-Ar diagram (Fig. 4c). The dark portions are equivalent to mixtures of irradiated and unirradiated small grains in various proportions (Fig. 4c), and their data plot along the tie line between irradiated and unirradiated small grains (gray points in Fig. 4c).

Thus, the two E chondrites experienced two exposure stages: exposure on the parent body with 2π geometry (parent-body exposure, Fig. 4a) and exposure in space with 4π geometry (space exposure, Fig. 4b). The concentration of $^{21}Ne_C$ produced during the parent body exposure is equivalent to $(^{21}Ne_C)_P$ (Fig. 4c). Assuming that irradiated small grains in Fig. 4c plot at points "A" and "M," respectively in Fig. 3, $(^{21}Ne_C)_P$ in Fig. 4c corresponds to that in Fig. 3. The concentration of $^{21}Ne_C$ produced during the space exposure is equivalent to $(^{21}Ne_C)_S$ (Fig. 4c), corresponding to that in Fig. 3. The correlation in Fig. 3 is attributed to the mixtures of irradiated and unirradiated small grains in various proportions (Fig. 4c). Solar-gas-poor samples in Fig. 3 may be dominated by unirradiated materials in Fig. 4c. Some of data in Fig. 3 fall far above the correlation lines, which may be due to higher $^{21}Ne_C$ production rate. It is discussed in detail in the next section.

The above interpretation applies to the samples measured by Wieler et al. (1989) and Pedroni (1991, 1992) without any further consideration. However, for our samples (Fig. 3), we did not measure noble gases separately in light and dark

portions. It is quite possible, therefore, that the samples are mixtures of light and dark portions, requiring a more complex interpretation. Admixture of the light portions to the dark portions is separated into two cases: admixture of unirradiated fragments and admixture of irradiated fragments. Addition of unirradiated fragments to the dark portions does not affect the correlation in Fig. 3 because the influence is the same as that of unirradiated small grains. Addition of irradiated fragments, on the other hand, results in an increase of $^{21}Ne_C$ concentrations and decrease of $^{36}Ar_S$ concentrations. Thus, the data points move to upper left from their original positions (gray points in Fig. 4c). As a result, the slope of the correlation line decreases and the ordinate intercept increases. Therefore, owing to the presence of irradiated fragments, the slope of the correlation line used for the calculation of heliocentric distances (next subsection) and $(^{21}Ne_C)_P$ may be underestimated, and $(^{21}Ne_C)_S$ may be overestimated. The slope and $(^{21}Ne_C)_P$ can be taken as lower limits and $(^{21}Ne_C)_S$ can be taken as an upper limit.

For the data presented in this work, we do not make the assumptions described in Nakashima et al. (2002). The assumptions are flawed in two respects. First, the irradiated grains are assumed to be located in the top cm of the regolith for several Ma. According to theoretical modeling of asteroid regolith (Housen et al. 1979), mixing on a 10 cm scale can occur within 1 Ma, indicating that the assumption is invalid. Second, the possibility that grains exposed exclusively to GCR on the parent body (and also in space) are mixed with irradiated and unirradiated grains is neglected.

Calculation of Heliocentric Distance

The heliocentric distance r_P we obtain here is the distance of the meteorite parent body from the Sun when constituents of the meteorite were exposed to solar wind. It can be obtained from the following equation:

$$r_P = \sqrt{\left(\frac{^{36}Ar_S}{^{21}Ne_C}\right)_L \Big/ \left(\frac{^{36}Ar_S}{^{21}Ne_C}\right)_P} \cdot R \qquad (1)$$

Here subscripts *P*, *L*, *S*, and *C* represent parent body, lunar, solar, and cosmogenic, respectively, and *R* is the correction factor for $^{21}Ne_C$ production rates, which is explained later. The calculation of r_P includes two assumptions: 1) the fluxes of energetic particles are the same during the lunar regolith exposure and parent body exposure, and 2) the ratio of the SW/SEP exposure duration to the parent body exposure age is similar for the Moon and meteorite parent body surfaces.

As found in Equation 1, r_P is obtained by comparison between the solar gas implantation rate of the meteorite and that of lunar samples. By using assumption (2), the solar gas implantation rate can be expressed as the ratio of solar gas concentration to the parent body exposure age deduced from $(^{21}Ne_C)_P$. However, the $^{21}Ne_C$ production rate, which is necessary for the calculation of the parent body exposure age, is not known due to lack of information about shielding conditions on the parent body. Therefore, the solar gas implantation rate is expressed as $(^{36}Ar_S/^{21}Ne_C)_P$, which is the inverse of the slope of the correlation line in Fig. 3. This is an upper limit and derived r_P is a lower limit, because the slope is a lower limit as mentioned in the previous section.

The $^{36}Ar_S$ and $^{21}Ne_C$ in Apollo soils and breccias show a correlation similar to those in Fig. 3 (Hintenberger et al. 1974). We use the slope of correlation line $(^{36}Ar_S/^{21}Ne_C)_L$ for the calculation of r_P. The $^{36}Ar/^{84}Kr$ ratios of the Apollo samples (2100 ± 300 on average) (Hintenberger et al. 1974) are comparable to that of the Sun (~2000) (Wieler 2002), suggesting no large diffusive loss of $^{36}Ar_S$. It is known that plagioclase from lunar soils lost some $^{21}Ne_C$ (e.g., Signer et al. 1977). Therefore, only plagioclase-poor mare samples are used for the $(^{36}Ar_S/^{21}Ne_C)_L$ calculation. The $^{21}Ne_C$ exposure ages of the Apollo mare samples agree (or closely agree) with those deduced from $^{38}Ar_C$ within errors (Hintenberger and Weber 1973), suggesting no large diffusive loss of $^{21}Ne_C$. Thus, it is unlikely that $^{36}Ar_S$ and $^{21}Ne_C$ losses affect the ratio of $(^{36}Ar_S/^{21}Ne_C)_L$ (=234) (Hintenberger et al. 1974; L. Schultz, personal communication).

Samples of the E chondrites, except for solar-gas-poor samples, show $(^3He/^{21}Ne)_C$ ratios lower than expected from the Bern plot (Eberhardt et al. 1966; Nishiizumi et al. 1980), suggesting preferential loss of ^3He_C from solar-gas-bearing samples. Also the possibility of $^{21}Ne_C$ loss from solar-gas-bearing samples cannot be excluded. If there is $^{21}Ne_C$ loss, the slope of the correlation line in Fig. 3 will decrease, but the ordinate intercept will remain unchanged. In light of these observations $(^{21}Ne_C)_P$ is a lower limit, $(^{36}Ar_S/^{21}Ne_C)_P$ is an upper limit, and the calculated r_P is a lower limit.

The *R* in Equation 1 is the ratio of $^{21}Ne_C$ production rate for lunar regolith exposure to that for parent body exposure. This ratio is used for correction of target element chemistry, because the $^{21}Ne_C$ production rate varies with target element chemistry. During the parent body exposure (Fig. 4a), the position of irradiated materials continuously changed in the 0–1 m depth range. Assuming the residence time of each material at any depth is the same down to 1 m, *R* can be estimated from the integrated $^{21}Ne_C$ production rate profile in lunar regolith and that in the parental regolith of the two meteorites. With the production rates given by Leya et al. (2001), the average chemical composition of Apollo mare samples (Goles et al. 1970; Wänke et al. 1970, 1971, 1972; LSPET 1973), and the chemical compositions of ALH 85119 and MAC 88136 (Wasson and Kallemeyn 1988; the average chemical composition of EL chondrites is applied for the two meteorites), *R* is calculated as 0.7.

The $^{36}Ar_S/^{21}Ne_C$ ratios are inversely related with grain size, because solar gas concentrations are inversely proportional to the grain sizes (e.g., Hintenberger and Weber

Table 2. $(^{36}Ar_S/^{21}Ne_C)_P$, $(^{21}Ne_C)_P$, and $(^{21}Ne_C)_S$ in ALH 85119 and MAC 88136[a].

Meteorite	$(^{36}Ar_S/^{21}Ne_C)_P$	$(^{21}Ne_C)_P$	$(^{21}Ne_C)_S$
		10^{-8} cm^3/g	
ALH 85119	<131	>1.28	<0.67
MAC 88136	<97.5	>1.67	<1.20

[a]$(^{36}Ar_S/^{21}Ne_C)_P$ is the solar gas implantation rate. $(^{21}Ne_C)_P$ and $(^{21}Ne_C)_S$ are concentrations of $^{21}Ne_C$ produced during the parent body exposure and space exposure, respectively. These three values are deduced as described in the "Interpretation and Calculation" section.

Table 3. Results of calculations[a].

Meteorite	r_P (AU)	T_P (Ma)	T_S (Ma)
ALH 85119	>1.1	>6.7	<2.2
MAC 88136	>1.3	>8.7	<3.9

[a]r_P is the distance of the meteorite parent body from the Sun when constituents of the meteorites were exposed to solar wind. T_P and T_S are the parent body exposure age and space exposure age, respectively.

1973). Thus, the difference between the average grain sizes of the Apollo samples and of the two E chondrites may affect r_P. Grain sizes of the Apollo samples used for $(^{36}Ar_S/^{21}Ne_C)_L$ calculation are 35–54 μm (Hintenberger et al. 1974), which are comparable with the assumed grain size of the dark portions in the two E chondrites (see previous subsection). Therefore, the influence of the grain-size difference on r_P is not considered.

Calculation of Parent Body Exposure Age

A lower limit for the parent body exposure age T_P is obtained from the $^{21}Ne_C$ production rate (P_P) and the lower limit of $(^{21}Ne_C)_P$ (Fig. 3; Table 2). During the parent body exposure, the locations of irradiated materials continuously change within the 0–1 m depth range (Fig. 4a), so we cannot determine the shielding depth. The shielding depth is assumed to be 40 g/cm^2, where P_P reaches a maximum (Leya et al. 2001). Thus, T_P ($(^{21}Ne_C)_P/P_P$) is a lower limit. P_P is obtained from the following equation:

$$P_P = 931[Mg] + 822[Na] + 343[Al] + 271[Si] + 45[Ca] + 7.3[Fe] + 7.4[Ni] \quad (2)$$

Here coefficients are the $^{21}Ne_C$ elemental production rates (in 10^{-11} cm^3/g · Ma) at the shielding depth of 40 g/cm^2, which are given by Leya et al. (2001), and [X] is concentration of element X as weight fraction. Concentrations of elements X are adopted from the chemical compositions of ALH 85119 and MAC 88136 (Wasson and Kallemeyn 1988; the average chemical composition of EL chondrites is applied for the two meteorites).

Calculation of Space Exposure Age

An upper limit for the space exposure age T_S is obtained by dividing the upper limit of $(^{21}Ne_C)_S$ by the $^{21}Ne_C$ production rate (P_S) (Fig. 3; Table 2). The shielding parameters $(^{22}Ne/^{21}Ne)_C$ for bulk ALH 85119 and MAC 88136 is assumed to be 1.11 (Patzer and Schultz 2001), corresponding to the average shielding parameter for chondrites. The $^{21}Ne_C$ production rates (in 10^{-10} cm^3/g · Ma) for the two meteorites in space are obtained from the equation given by Schultz and Freundel (1985) for the average shielding:

$$P_S = 163[Mg] + 60[Al] + 32[Si] + 22[S] + 7[Ca] + 2.1[Fe+Ni] \quad (3)$$

Again, [X] is the concentration of element X as weight fraction.

RESULTS OF CALCULATIONS AND DISCUSSION

Table 3 shows the calculated r_P, T_P, and T_S for ALH 85119 and MAC 88136.

Exposure Ages

Based on the arguments presented earlier we consider the parent body exposure age T_P is a lower limit. This argument is reinforced by the observation that the "true" irradiated small grains (Fig. 4c) may contain higher concentrations of solar and cosmogenic gases than the samples represented by points "A" and "M" in Fig. 3. Langevin and Maurette (1980) inferred from their regolith evolution model that parent body exposure ages are ~10 Ma and ~1 Ma for constituents of regoliths on strong and weak asteroids, respectively. For both E chondrites T_P are >7 Ma, which suggests strong parent bodies for both.

In our exposure scenarios (Fig. 4), we have assumed that all the regolith materials became shielded from all energetic particles including GCR after the parent body exposure. However, it is also possible that material was reexposed only to GCR due to reexcavation. If this occurred, only the $^{21}Ne_C$ concentration would increase in a similar way as during space exposure. This means that $(^{21}Ne_C)_S$ may include $^{21}Ne_C$ produced during a reexposure on the parent body, and the $^{21}Ne_C$ produced during space exposure is actually lower than the $(^{21}Ne_C)_S$ determined by our approach. It follows that T_S is an upper limit, as already concluded in the previous section. Even if the re-exposure did occur, r_P is not changed, because $(^{21}Ne_C)_P$ and $^{36}Ar_S$ are not changed.

Assumptions for the r_P Calculation

In the calculation of r_P, we made two assumptions: 1) that fluxes of energetic particles are the same during lunar regolith exposure and parent body exposure, and 2) that the ratio of the SW/SEP exposure duration to parent body exposure age, estimated from GCR-produced $^{21}Ne_C$, is similar for the Moon and meteorite parent body surfaces. These two assumptions

need to be discussed. As for the first assumption, Geiss (1973) and Wieler (1997) suggested that the SW flux ~4 Ga ago was higher than today. Below we discuss the consequences of SW exposure with higher flux in the case of the E chondrites. The $(^{40}Ar/^{36}Ar)_{trapped}$ ratios of lunar samples are indicators of the time when SW implantation occurred (Eugster et al. 1983). They vary among the Apollo samples (0.42–7.4) (Hintenberger and Weber 1973; Hintenberger et al. 1974), which suggests that the Apollo samples consist of soils exposed to SW at various times (~0–3 Ga) (cf. Eugster et al. 2001). Thus, the $(^{36}Ar_S/^{21}Ne_C)_L$ ratio deduced from the Apollo samples can be taken as the long-term average flux of solar gases. If the flux of solar gases implanted to the E chondrites was higher than this long-term average flux, the result underestimates r_P due to a higher $(^{36}Ar_S/^{21}Ne_C)_P$ ratio. In this case r_P is a lower limit. Thus, the results are not changed even if the SW flux during the parent body exposure was higher than the average SW flux: r_P is a lower limit. Regarding the second assumption, by using this assumption, Anders (1975) and Wieler et al. (1989) inferred that meteorite parent bodies are located in the asteroid belt. This is also inferred from reflectance spectra (e.g., Pieters and McFadden 1994) and calculations of meteoroid trajectories (Lowrey 1971; Levin et al. 1976; Wetherill 1976; Ballabh et al. 1978; Brown et al. 2000), which also indicate that meteorites originate in the asteroid belt.

Comparison between Formation Regions of E Chondrites and r_P

It is inferred from the mineralogy and chemistry of E chondrites that they formed in regions within 1.4 AU (Larimer and Anders 1967; Baedecker and Wasson 1975; Sears 1980; Kallemeyn and Wasson 1986; Shukolyukov and Lugmair 2004). Our results indicate that the regolith exposure occurred at the heliocentric distances of >1.1 AU for ALH 85119 and >1.3 AU for MAC 88136. The similarity in presumed formation location and exposure location may imply that the heliocentric distances of E chondrite parent bodies were relatively constant from their initial formation stage up to the time of their exposure to the Sun.

Data Deviations from the Correlation Line in Figure 3

Here we discuss the data plotting far above the correlation lines (marked by arrows in Fig. 3). There are two possible explanations for the large deviations: 1) preferential solar gas loss and 2) higher $^{21}Ne_C$ production rate.

With preferential solar gas loss, if $^{36}Ar_S$ loss occurs, the data would shift to the left and would plot above the correlation line (Fig. 3). This must be accompanied by the preferential loss of $^{20}Ne_S$, resulting in lower $(^{20}Ne/^{36}Ar)_S$ ratios relative to those not having experienced $^{20}Ne_S$ loss. However, the $(^{20}Ne/^{36}Ar)_S$ ratios of the samples with the large deviations are comparable to those of the others, indicating no larger loss of $^{20}Ne_S$ or $^{36}Ar_S$.

With a higher $^{21}Ne_C$ production rate, the $^{21}Ne_C$ production rate depends on target element chemistry and shielding conditions. The main target element for $^{21}Ne_C$ production is Mg, which is mainly present in enstatite and forsterite in E chondrites. It is possible that the samples with the large deviations are dominated by enstatite and forsterite. Another possibility is that the samples include irradiated small grains and/or fragments located at a depth with higher $^{21}Ne_C$ production rate. We have assumed that irradiated materials are mixed continuously in the 0–1 m depth range during the parent body exposure (Fig. 4a). However, regolith mixing is an inherently random process. Therefore, it is possible that part of the irradiated materials spent most of their parent body exposure time at a depth having a higher $^{21}Ne_C$ production rate. We regard "higher $^{21}Ne_C$ production rate" as the most likely explanation for data plotting above the correlation lines.

Small deviations from the correlation lines in Fig. 3 may be due to small diffusive losses of $^{21}Ne_C$ and/or $^{36}Ar_S$ or to different $^{21}Ne_C$ production rate by variations in the chemical compositions of samples and/or different shielding condition during the parent body exposure.

CONCLUSIONS

Concentrations and isotopic ratios of noble gases in the two E chondrites ALH 85119 and MAC 88136 were determined in order to calculate heliocentric distances of the parent bodies, parent body exposure ages, and space exposure ages. The parent body exposure ages are longer than 6.7 Ma and 8.7 Ma for ALH 85119 and MAC 88136, respectively, while upper limits of the space exposure ages are 2.2 Ma and 3.9 Ma. The heliocentric distances at which the regolith was exposed to the Sun are greater than 1.1 AU and 1.3 AU. They are not different from the formation regions of E chondrites (<1.4 AU). This may imply that heliocentric distances of E chondrites have been relatively constant from their formation stage to the stage of exposure to the Sun.

Acknowledgments–We thank Dr. M. W. Caffee, Dr. R. Wieler, and an anonymous reviewer for their critical comments and helpful reviews. We also thank the NASA Johnson Space Center for providing samples of ALH 85119 and MAC 88136, and Dr. U. Ott for constructive comments.

Editorial Handling—Dr. Marc Caffee

REFERENCES

Anders E. 1975. Do stony meteorites come from comets? *Icarus* 24: 363–371.

Baedecker P. A. and Wasson J. T. 1975. Elemental fractionation

among enstatite chondrites. *Geochimica et Cosmochimica Acta* 39:735–765.

Ballabh G. M., Bhatnager A., and Bhandari N. 1978. The orbit of the Dhajala meteorite. *Icarus* 33:361–367.

Benkert J.-P., Baur H., Signer P., and Wieler R. 1993. He, Ne, and Ar from the solar wind and solar energetic particles in lunar ilmenites and pyroxenes. *Journal of Geophysical Research* 98: 13,147–13,162.

Brown P. G., Hildebrand A. R., Zolensky M. E., Grady M. M., Clayton R. N., Mayeda T. K., Tagliaferri E., Spalding R., MacRae N. D., Hoffman E. L., Mittlefehldt D. W., Wacker J. F., Bird J. A., Campbell M. D., Carpenter R., Gingerich H., Glatiotis M., Greiner E., Mazur M. J., McCausland P. J. A., Plotkin H., and Mazur T. R. 2000. The fall, recovery, orbit, and composition of the Tagish Lake meteorite: A new type of carbonaceous chondrite. *Science* 290:320–325.

Busemann H., Baur H., and Wieler R. 2000. Primordial noble gases in "Phase Q" in carbonaceous and ordinary chondrites studied by closed-system stepped etching. *Meteoritics & Planetary Science* 35:949–973.

Clayton R. N. and Mayeda T. K. 1985. Oxygen isotopes in chondrules from enstatite chondrites: Possible identification of a major nebular reservoir (abstract). 16th Lunar and Planetary Science Conference. pp. 142–143.

Clayton R. N., Mayeda T. K., and Rubin A. E. 1984. Oxygen isotopic compositions of enstatite chondrites and aubrites. *Journal of Geophysical Research* 89:C245–C249.

Eberhardt P., Geiss J., and Grögler N. 1965. Further evidence on the origin of trapped gases in the meteorite Khor Temiki. *Journal of Geophysical Research* 70:4375–4378.

Eberhardt P., Geiss J., Graf H., Grögler N., Mendia M. D., Mörgeli M., Schwaller H., Stettler A., Krähenbühl U., and von Gunten H. R. 1972. Trapped solar wind noble gases in Apollo 12 lunar fines 12001 and Apollo 11 breccia 10046. Proceedings, 3rd Lunar Science Conference. pp. 1821–1856.

Eberhardt P., Eugster O., Geiss J., and Marti K. 1966. Rare gas measurements in 30 stone meteorites. *Zeitschrift für Naturforschung A* 21:414–426.

Eugster O., Geiss J., and Grögler N. 1983. Dating of early regolith exposure and the evolution of trapped $^{40}Ar/^{36}Ar$ with time (abstract). 14th Lunar and Planetary Science Conference. pp. 177–178.

Eugster O., Terribilini D., Polnau E., and Kramers J. 2001. The antiquity indicator argon-40/argon-36 for lunar surface samples calibrated by uranium-235–xenon-136 dating. *Meteoritics & Planetary Science* 36:1097–1115.

Geiss J. 1973. Solar wind composition and implications about the history of the solar system. Proceedings, 13th International Cosmic Ray Conference. pp. 3375–3398.

Goles G. G., Randle K., Osawa M., Lindstrom D. J., Jerome D. Y., Steinborn T. L., Beyer R. L., Martin M. R., and McKay S. M. 1970. Interpretations and speculations on elemental abundances in lunar samples. Proceedings, Apollo 11 Lunar Science Conference. pp. 1177–1194.

Goswami J. N., Lal D., and Wilkening L. L. 1984. Gas-rich meteorites: Probes for the particle environment and dynamical processes in the inner solar system. *Space Science Reviews* 37: 111–159.

Hintenberger H. and Weber H. W. 1973. Trapped rare gases in lunar fines and breccias. Proceedings, 4th Lunar Conference. pp. 2003–2019.

Hintenberger H., Weber H. W., and Schultz L. 1974. Solar, spallogenic, and radiogenic rare gases in Apollo 17 soils and breccias. Proceedings, 5th Lunar Conference. pp. 2002–2022.

Housen K. R. and Wilkening L. L. 1982. Regoliths on small bodies in the solar system. *Annual Reviews of Earth and Planetary Sciences* 10:355–376.

Housen K. R., Wilkening L. L., Chapman C. R., and Greenberg R. 1979. Asteroidal regolith. *Icarus* 39:317–351.

Ivanov A. V., Ul'Ianov A. A., Ustinov V. I., Skripnik A. Ia., and Gavrilov E. Ia. 1987. Isotopic compositions of oxygen in samples of the Kaidun meteorite. *Meteoritika* 46:40–44.

Keil K. 1982. Composition and origin of chondrite breccias. Lunar Planetary Institute Technical Report #82-02. Houston, Texas: Lunar and Planetary Institute. pp. 65–83.

Kallemeyn G. W. and Wasson J. T. 1986. Composition of enstatite (EH3, EH4, 5, and EL6) chondrites: Implications regarding their formation. *Geochimica et Cosmochimica Acta* 50:2153–2164.

Lal D. and Rajan R. S. 1969. Observations on space irradiation of individual crystals of gas-rich meteorites. *Nature* 223:269–271.

Langevin Y. and Maurette M. 1980. A model for small body regolith evolution: The critical parameters (abstract). Proceedings, 11th Lunar and Planetary Science Conference. pp. 602–604.

Larimer J. W. and Anders E. 1967. Chemical fractionation in meteorites—II. Abundance patterns and their interpretation. *Geochimica et Cosmochimica Acta* 31:1239–1270.

Levin B. J., Simonenko A. N., and Anders E. 1976. Farmington meteorite: A fragment of Apollo asteroid? *Icarus* 28:307–324.

Leya I., Neumann S., Wieler R., and Michel R. 2001. The production of cosmogenic nuclides by GCR-particles for 2π exposure geometries. *Meteoritics & Planetary Science* 36:1547–1561.

Lowrey B. E. 1971. Orbital evolution of Lost City meteorite. *Journal of Geophysical Research* 76:4084–4089.

Lunar Sample Preliminary Examination Team (LSPET). 1973. Apollo 17 lunar samples: Chemical and petrographic description. *Science* 182:659–671.

Lugmair G. W. and Shukolyukov A. 1998. Early solar system time scales according to ^{53}Mn-^{53}Cr systematics. *Geochimica et Cosmochimica Acta* 62:2863–2886.

Mayeda T. K. and Clayton R. N. 1980. Oxygen isotopic compositions of aubrites and some unique meteorites. Proceedings, 11th Lunar and Planetary Science Conference. pp. 1145–1151.

Nakamura T., Noguchi T., Zolensky M. E., and Tanaka M. 2003. Mineralogy and noble-gas signatures of the carbonate-rich lithology of the Tagish Lake carbonaceous chondrite: Evidence for an accretionary breccia. *Earth and Planetary Science Letters* 207:83–101.

Nakashima D., Nakamura T., Sekiya M., and Takaoka N. 2002. Cosmic-ray exposure age and heliocentric distance of the parent body of H chondrites Yamato-75029 and Tsukuba. *Antarctic Meteorite Research* 15:97–113.

Newton J., Franchi I. A., and Pillinger C. 2000. The isotope record in enstatite meteorites. *Meteoritics & Planetary Science* 35:689–698.

Nishiizumi K., Regnier S., and Marti K. 1980. Cosmic ray exposure ages of chondrites, pre-irradiation, and constancy of cosmic ray flux in the past. *Earth and Planetary Science Letters* 50:156–170.

Okazaki R., Takaoka N., Nakamura T., and Nagao K. 2000. Cosmic-ray exposure ages of enstatite chondrites. *Antarctic Meteorite Research* 13:153–169.

Patzer A. and Schultz L. 2001. Noble gases in enstatite chondrites. I: Exposure ages, pairing, and weathering effects. *Meteoritics & Planetary Science* 36:947–961.

Patzer A. and Schultz L. 2002. Noble gases in enstatite chondrites. II: The trapped component. *Meteoritics & Planetary Science* 37: 601–612.

Patzer A., Franke L., and Schultz L. 2001. New noble gas data of four enstatite chondrites and Zaklodzie (abstract). *Meteoritics & Planetary Science* 36:A157.

Pieters C. M. and McFadden L. A. 1994. Meteorite and asteroid

reflectance spectroscopy: Clues to early solar system. *Annual Reviews of Earth and Planetary Sciences* 22:457–497.

Pedroni A. 1991. Precompaction irradiation of the howarditic regolith breccia Kapoeta (abstract). 22nd Lunar and Planetary Science Conference. pp. 1047–1048.

Pedroni A. 1992. The irradiation history of the H-chondritic regolith breccia Acfer 111 (abstract). *Meteoritics* 27:273.

Pellas P. 1972. Irradiation history of grain aggregates in ordinary chondrites, possible clues to the advanced stages of accretion. In *From plasma to planet,* edited by Elvius A. New York: Wiley. pp. 65–92.

Pellas P., Poupeau G., Lorin J. C., Reeves H., and Andouze J. 1969. Primitive low-energy particle irradiation of meteoritic crystals. *Nature* 223:272–274.

Rajan R. S. 1974. On the irradiation history and origin of gas-rich meteorites. *Geochimica et Cosmochimica Acta* 38:777–788.

Schultz L. 1973. Die Bestrahlungsgeschichte Xenolithischer Chondrite. Habilitationsschrift, ETH, Zuerich.

Schultz L. and Freundel M. 1985. On the production rate of ^{21}Ne in ordinary chondrites. In *Isotopic ratios in the solar system,* edited by Centre National d'Etudes Spatiales. Toulouse: Cepadues-Editions. pp. 27–33.

Schultz L., Signer P., Lorin J. C., and Pellas P. 1972. Complex irradiation history of the Weston chondrite. *Earth and Planetary Science Letters* 15:403–410.

Sears D. W. G. 1980. Formation of E chondrites and aubrites—A thermodynamic model. *Icarus* 43:184–202.

Shukolyukov A. and Lugmair G. W. 2004. Manganese-chromium systematics of enstatite meteorites. *Geochimica et Cosmochimica Acta* 68:2875–2888.

Signer P. 1964. Primordial rare gases in meteorites. In *The origin and evolution of atmospheres and oceans,* edited by Brancazio P. J. and Cameron A. G. W. New York: Wiley. pp. 183–190.

Signer P., Baur H., Derksen U., Etique P., Funk H., Horn P., and Wieler R. 1977. Helium, neon, and argon records of lunar soil evolution. Proceedings, 8th Lunar Science Conference. pp. 3657–3683.

Suess H. E., Wänke H., and Wlotzka F. 1964. On the origin of gas rich meteorites. *Geochimica et Cosmochimica Acta* 28:209–233.

Walker R. M. 1980. Nature of the fossil evidence: Moon and meteorites. In *The ancient Sun: Fossil record in the Earth, Moon, and meteorites,* edited by Pepin R. O., Eddy J. A., and Merrill R. B. New York: Pergamon Press. pp. 11–28.

Wänke H. 1965. Der Sonnenwind als Quelle der Uredelgase in Steinmeteoriten. *Zeitschrift für Naturforschung A* 20:747–765.

Wänke H., Rieder R., Baddenhausen H., Spettel B., Teschke F., Quijano-Rico M., and Balacescu A. 1970. Major and trace elements in lunar material. Proceedings, Apollo 11 Lunar Science Conference. pp. 1719–1727.

Wänke H., Wlotzka F., Baddenhausen H., Balacescu A., Spettel B., Teschke F., Jagoutz E., Kruse H., Quijano-Rico M., and Rieder R. 1971. Apollo 12 samples: Chemical composition and its relation to sample locations and exposure ages and studies on lunar metal particles. Proceedings, 2nd Lunar Science Conference. pp. 1187–1208.

Wänke H., Baddenhausen H., Balacescu A., Teschke F., Spettel B., Dreibus G., Palme H., Quijano-Rico M., Kruse H., Wlotzka F., and Begemann F. 1972. Multielement analyses of lunar samples and some implications of the results. Proceedings, 3rd Lunar Science Conference. pp. 1251–1268.

Wetherill G. W. 1976. Where do the meteorites come from? A re-evaluation of the Earth-crossing Apollo objects as sources of chondritic meteorites. *Geochimica et Cosmochimica Acta* 40: 1297–1317.

Wilkening L. L. 1971. Particle track and studies and the origin of gas-rich meteorites. Nininger Meteorite Award Paper. Tempe, Arizona: Arizona State University.

Wasson J. T. and Kallemeyn G. W. 1988. Compositions of chondrites. *Philosophical Transactions of the Royal Society of London A* 325:535–544.

Wieler R. 1997. Why are SEP noble gases so abundant in extraterrestrial samples? (abstract). Proceedings, 28th Lunar and Planetary Science Conference. pp. 1551–1552.

Wieler R. 2002. Noble gases in the solar system. In *Noble gases in geochemistry and cosmochemistry,* edited by Porcelli D., Ballentine C. J., and Wieler R. Washington, D.C.: Mineralogical Society of America. pp. 21–70.

Wieler R., Baur H., Pedroni A., Signer P., and Pellas P. 1989. Exposure history of the regolithic chondrite Fayetteville: I. Solar-gas-rich matrix. *Geochimica et Cosmochimica Acta* 53:1441–1448.

APPENDIX

Table A1. Concentrations and isotopic ratios of noble gases in small samples of ALH 85119.

Sample	Mass (mg)	^{4}He (10^{-8} cm^3/g)	^{3}He/^{4}He	^{20}Ne (10^{-8} cm^3/g)	^{20}Ne/^{22}Ne	^{21}Ne/^{22}Ne	^{36}Ar (10^{-8} cm^3/g)	^{38}Ar/^{36}Ar	^{40}Ar/^{36}Ar	^{84}Kr (10^{-9} cm^3/g)	^{132}Xe (10^{-9} cm^3/g)
A1	2.2	119,779	0.000360 ± 0.000008	2362	12.1 ± 0.1	0.0359 ± 0.0009	95.6	0.187 ± 0.001	70.4 ± 0.2	3.50	6.32
A2	1.1	134,812	0.000340 ± 0.000006	2662	12.1 ± 0.1	0.0354 ± 0.0009	119	0.187 ± 0.001	49.3 ± 0.2	3.89	6.81
A3	1.1	1286	0.002913 ± 0.000118	1.11	1.28 ± 3.16	0.698 ± 0.149	7.89	0.197 ± 0.002	629 ± 17	1.82	2.73
A4	0.7	11,839	0.000666 ± 0.000014	246	12.0 ± 0.1	0.0680 ± 0.0042	11.1	0.195 ± 0.001	407 ± 8	0.691	1.18
A5	0.7	17,429	0.000505 ± 0.000009	385	11.8 ± 0.1	0.0583 ± 0.0022	23.0	0.190 ± 0.001	321 ± 3	2.69	4.01
A6	0.7	61,484	0.000366 ± 0.000009	1203	12.1 ± 0.1	0.0384 ± 0.0011	51.6	0.188 ± 0.000	92.3 ± 0.5	3.66	8.97
A7	0.7	178,894	0.000372 ± 0.000010	3018	12.0 ± 0.1	0.0372 ± 0.0010	134	0.188 ± 0.000	53.5 ± 0.3	3.56	6.72
A8	1.6	179,854	0.000343 ± 0.000007	3923	12.1 ± 0.0	0.0353 ± 0.0010	187	0.187 ± 0.000	42.7 ± 0.3	5.49	6.86
A9	1.7	136,996	0.000358 ± 0.000004	2707	12.0 ± 0.0	0.0382 ± 0.0011	122	0.188 ± 0.001	54.3 ± 0.5	6.30	8.59
A10	1.3	119,789	0.000343 ± 0.000010	2613	12.1 ± 0.0	0.0353 ± 0.0010	117	0.187 ± 0.001	49.1 ± 0.6	4.20	5.43
A11	1.3	54,945	0.000377 ± 0.000007	851	12.0 ± 0.1	0.0431 ± 0.0013	48.3	0.189 ± 0.001	152 ± 1	7.01	11.0
A12	0.8	167,136	0.000354 ± 0.000006	2736	12.1 ± 0.0	0.0361 ± 0.0010	120	0.188 ± 0.001	61.4 ± 1.0	6.25	9.29
A13	0.8	129,330	0.000334 ± 0.000004	2992	12.1 ± 0.1	0.0360 ± 0.0010	138	0.187 ± 0.001	44.2 ± 0.9	4.60	4.56
A14	1.0	49,706	0.000352 ± 0.000006	1162	12.3 ± 0.1	0.0372 ± 0.0012	44.5	0.188 ± 0.001	57.2 ± 2.2	2.00	2.00
A15	1.9	33,271	0.000440 ± 0.000004	600	12.6 ± 0.0	0.0368 ± 0.0004	25.8	0.191 ± 0.000	49.6 ± 1.0	2.44	6.48
A16	0.7	177,119	0.000392 ± 0.000003	4168	12.5 ± 0.0	0.0354 ± 0.0005	161	0.185 ± 0.003	31.2 ± 0.5	3.98	8.80
A17	1.0	283,105	0.000333 ± 0.000002	4991	12.5 ± 0.0	0.0342 ± 0.0003	181	0.184 ± 0.000	27.7 ± 0.3	5.65	12.9
A18	1.0	130,784	0.000355 ± 0.000003	3281	12.5 ± 0.0	0.0400 ± 0.0005	121	0.186 ± 0.000	39.6 ± 0.5	4.28	10.4
A19	0.6	127,258	0.000351 ± 0.000003	2581	12.5 ± 0.0	0.0362 ± 0.0005	94.8	0.185 ± 0.000	41.8 ± 0.9	2.71	6.12
A20	0.8	176,044	0.000392 ± 0.000003	3878	12.5 ± 0.0	0.0427 ± 0.0004	136	0.186 ± 0.000	32.7 ± 0.5	4.05	8.75
A21	0.4	189,236	0.000332 ± 0.000003	4411	12.6 ± 0.0	0.0350 ± 0.0004	160	0.186 ± 0.001	33.6 ± 0.9	4.80	12.6

The errors in gas concentrations are less than 4%, 255%, 5%, 10%, and 9% for ^{4}He, ^{20}Ne, ^{36}Ar, ^{84}Kr, and ^{132}Xe, respectively, and include all errors of experiments, standards, and so forth.

Table A2. Concentrations and isotopic ratios of noble gases in small samples of MAC 88136.

Sample	Mass (mg)	^{4}He (10^{-8} cm^3/g)	^{3}He/^{4}He	^{20}Ne (10^{-8} cm^3/g)	^{20}Ne/^{22}Ne	^{21}Ne/^{22}Ne	^{36}Ar (10^{-8} cm^3/g)	^{38}Ar/^{36}Ar	^{40}Ar/^{36}Ar	^{84}Kr (10^{-9} cm^3/g)	^{132}Xe (10^{-9} cm^3/g)
M1	1.1	261,839	0.000298 ± 0.000004	2433	11.6 ± 0.1	0.0374 ± 0.0012	89.5	0.191 ± 0.000	58.0 ± 0.3	2.04	2.07
M2	0.9	394,145	0.000308 ± 0.000005	4162	11.8 ± 0.1	0.0357 ± 0.0011	160	0.190 ± 0.001	35.7 ± 0.2	2.67	2.24
M3	0.8	421,575	0.000316 ± 0.000004	4596	11.8 ± 0.1	0.0368 ± 0.0010	173	0.190 ± 0.001	39.7 ± 0.2	2.84	2.43
M4	0.6	244,501	0.000330 ± 0.000006	2195	11.6 ± 0.1	0.0438 ± 0.0012	84.8	0.192 ± 0.001	87.3 ± 0.4	1.98	1.92
M5	0.5	232,375	0.000320 ± 0.000003	1930	11.5 ± 0.1	0.0422 ± 0.0010	65.6	0.191 ± 0.001	77.1 ± 0.6	1.25	1.26
M6	0.9	296,369	0.000304 ± 0.000003	2729	11.7 ± 0.1	0.0389 ± 0.0012	98.6	0.191 ± 0.001	73.6 ± 0.3	2.67	2.67
M7	0.8	305,870	0.000307 ± 0.000003	2973	11.4 ± 0.1	0.0390 ± 0.0011	102	0.191 ± 0.001	56.8 ± 0.3	2.20	2.09
M8	0.6	357,705	0.000309 ± 0.000006	3324	11.5 ± 0.1	0.0385 ± 0.0012	109	0.191 ± 0.000	69.4 ± 0.3	2.32	2.36
M9	0.8	161,737	0.000310 ± 0.000005	1592	11.6 ± 0.1	0.0384 ± 0.0012	67.5	0.192 ± 0.001	101 ± 1	4.69	2.97
M10	0.7	170,259	0.000303 ± 0.000007	1720	11.5 ± 0.1	0.0392 ± 0.0012	66.3	0.191 ± 0.001	82.9 ± 1.9	2.96	1.59
M11	0.5	1245	0.003734 ± 0.000282	5.68	3.90 ± 1.80	0.453 ± 0.060	n.m.	n.m.	n.m.	n.m.	n.m.
M12	1.0	118,497	0.000318 ± 0.000005	1212	11.6 ± 0.1	0.0400 ± 0.0012	58.6	0.191 ± 0.001	123 ± 1	6.28	7.67
M13	1.0	280,041	0.000307 ± 0.000002	2735	12.0 ± 0.0	0.0384 ± 0.0007	92.0	0.188 ± 0.000	65.3 ± 0.6	2.60	2.37
M14	0.5	220,220	0.000310 ± 0.000003	1968	12.0 ± 0.1	0.0399 ± 0.0008	68.7	0.188 ± 0.001	72.5 ± 1.4	2.05	1.88
M15	0.3	287,126	0.000304 ± 0.000003	2663	11.9 ± 0.1	0.0391 ± 0.0006	92.9	0.190 ± 0.001	71.6 ± 1.7	2.68	2.40
M16	0.9	196,948	0.000351 ± 0.000003	2201	11.7 ± 0.0	0.0557 ± 0.0007	82.2	0.186 ± 0.001	67.4 ± 0.7	2.33	2.64
M17	1.0	295,785	0.000315 ± 0.000002	2750	11.9 ± 0.0	0.0376 ± 0.0004	90.3	0.188 ± 0.001	57.4 ± 0.6	2.66	3.15
M18	1.2	193,328	0.000326 ± 0.000003	1878	11.9 ± 0.0	0.0393 ± 0.0007	67.1	0.189 ± 0.001	59.3 ± 0.7	1.91	2.48
M19	0.4	249,344	0.000318 ± 0.000002	2513	11.9 ± 0.1	0.0423 ± 0.0003	87.6	0.188 ± 0.001	59.9 ± 1.3	2.07	2.48
M20	0.7	302,182	0.000315 ± 0.000003	2849	12.0 ± 0.0	0.0376 ± 0.0004	94.2	0.190 ± 0.001	58.2 ± 0.8	2.31	2.68

The errors in gas concentrations are less than 9%, 53%, 3%, 10%, and 10% for ^{4}He, ^{20}Ne, ^{36}Ar, ^{84}Kr, and ^{132}Xe, respectively, and include all errors of experiments, standards, and so forth.
n.m. = not measured.